High-Yield Sorting of Small-Diameter Carbon Nanotubes for Solar Cells and Transistors

Huiliang Wang,[†,∥] Ghada I. Koleilat,[‡,∥] Peng Liu,[§] Gonzalo Jiménez-Osés,[§] Ying-Chih Lai,[‡,⊥] Michael Vosgueritchian,[‡] Ya Fang,[†] Steve Park,[†] Kendall N. Houk,[§] and Zhenan Bao[‡,*]

[†]Department of Materials Science & Engineering, Stanford University, Stanford, California 94305, United States, [‡]Department of Chemical Engineering, Stanford University, Stanford, California 94305, United States, [§]Department of Chemistry and Biochemistry, University of California, Los Angeles, California 90095, United States, and [⊥]Graduate Institute of Electronics Engineering, National Taiwan University, Taipei 10617, Taiwan, Republic of China. [∥]These authors contributed equally to this work.

ABSTRACT We describe herein a high-yield method to selectively disperse semiconducting CoMoCAT (CO disproportionation on Co—Mo catalysts) single-walled carbon nanotubes (SWNTs) with regioregular poly(3-alkylthiophenes) polymers. We observed that the dispersion yield was directly related to the length of the polymer's alkyl side chains. Molecular dynamics simulations in explicit toluene (real toluene molecules) indicate that polythiophenes with longer alkyl side chains bind strongly to SWNTs, due to the increased overall surface contact area with the nanotube. Furthermore, the sorting process selectively enriches smaller-diameter CoMoCAT SWNTs with larger bandgaps, which is ideal for solar cell applications. Compared to the larger diameter sorted HiPco (High-Pressure CO) SWNTs, solar cells fabricated using our sorted CoMoCAT SWNTs demonstrated higher open-circuit voltage (V_{oc}) and infrared external quantum efficiency (EQE). The V_{oc} achieved is the highest reported for solar cells based on SWNT absorbers under simulated AM1.5 solar illumination. Additionally, we employed the sorted CoMoCAT SWNTs to fabricate thin film transistors with excellent uniformity and device performance.

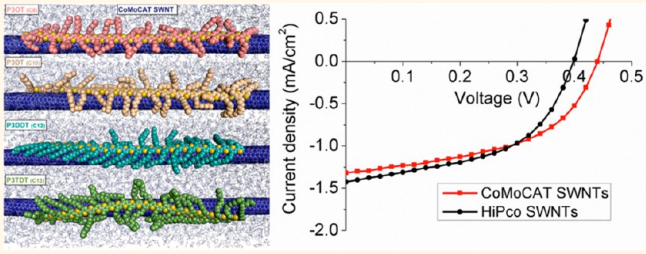

KEYWORDS: carbon nanotubes · small-diameter · high yield · solar cells · transistors

Single-walled carbon nanotubes (SWNTs) have been widely studied in the field of electronics and optoelectronics due to their high carrier mobility,[1,2] strong absorptivity[3] and their direct bandgaps. Applications include thin film transistors,[4,5] logic circuits,[6] solar cells[7,8] and photodetectors.[9] However, the as-synthesized SWNTs are typically mixtures of tubes with various chiralities, with approximately one-third metallic and the remaining two-third semiconducting. They also have a wide range of diameters and bandgaps, which have significant impact on device performance. As a reference, arc-discharge SWNTs have diameters of 1.2—1.7 nm, HiPco SWNTs have diameters of 0.8—1.1 nm, while CoMoCATs SWNTs have smaller diameters of 0.7—0.9 nm. Until now, great progress has been made on sorting SWNTs by solution-based noncovalent functionalization of SWNTs. This approach has the advantage of not significantly altering the SWNTs' electronic properties. Examples of this approach include density gradient centrifugation,[10] sorting by DNAs,[11] gel chromatography,[12] and selective dispersion by conjugated polymers.[13—15] However, most of these processes suffer from low-yield, lengthy procedures or difficulty in removing insulating sorting reagents. Sorting of SWNTs by conjugated polymers is of particular interest because of its simplicity, high selectivity and high-yield.[13,14]

Recent effort has been directed to conjugated polymer sorting of larger-diameter arc-discharge SWNTs due to their potentially superior electronic properties.[15—17] However, less work has been done on conjugated polymer sorting of CoMoCAT SWNTs, the smallest-diameter mass-produced SWNTs. It has been predicted that CoMoCAT SWNTs have lower mobilities[18] and larger Schottky barriers which together yields lower on-current density in field-effect transistors.[19] On the other hand,

* Address correspondence to zbao@stanford.edu.

Received for review December 6, 2013 and accepted January 31, 2014.

Published online 10.1021/nn406256y

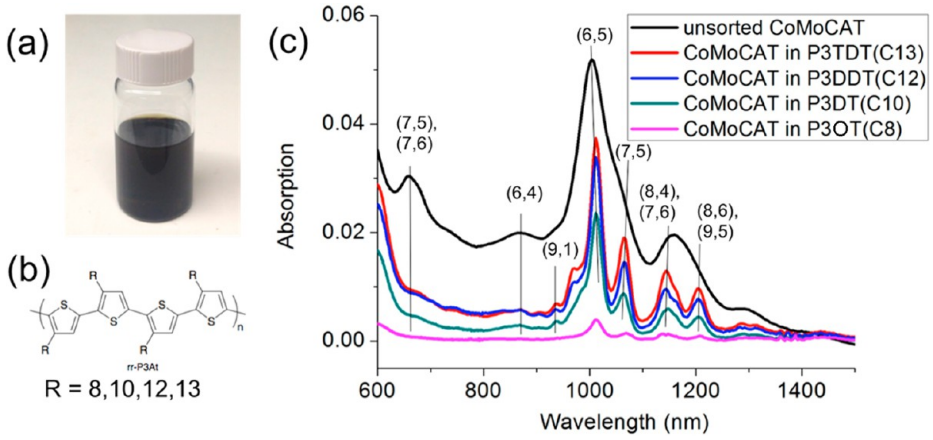

Figure 1. (a) Sorted CoMoCAT carbon nanotube solutions by P3DDT; (b) polymer structure of polythiophenes with different side chains. (c) Optical Absorbance spectra comparing unsorted CoMoCAT SWNTs dispersed in NMP to the ones sorted by polythiophenes in toluene.

CoMoCAT SWNTs could in principle be beneficial as part of the active absorbing layer in solar cells because their wider bandgap would allow the formation of an improved type-II heterojunction with C_{60} acceptors.[20] A similar type-II heterojunction using smaller-SWNTs as an acceptor and P3HT as a donor has been demonstrated.[21] However, sorting of semiconducting CoMoCAT SWNTs has only been achieved in low yields using poly(9,9-dioctylfluorenyl-2,7-diyl) (PFO),[13] and PFO-BPy,[22] which limits their scalability for industrial applications. Arnold *et al.* used the sorted (7,5) (0.82 nm in diameter) CoMoCAT tubes[13] together with C_{60} as the active layers in solar cells.[20] It is expected that even smaller diameter SWNTs will further improve charge separation and increase open circuit voltage (V_{oc}).

Herein, we report the selective dispersion of small-diameter semiconducting CoMoCAT SWNTs using regioregular poly(3-alkylthiophene)s (rr-P3ATs). We observed that rr-P3ATs selectively enriched CoMoCAT SWNTs with diameters less than 0.76 nm. By increasing the length of the alkyl side chains, we were able to increase the dispersion yield. As a result, thicker films can be prepared to allow more light absorption for solar cell devices. Molecular dynamics simulations in presence of toluene solvent molecules indicated that the increased yield is due to the higher contact surface area between longer side chain polymers and SWNTs. In comparison with poly(3-dodecylthiophene-2,5-diyl) (P3DDT) sorted larger-diameter HiPco SWNTs, P3DDT-sorted CoMoCAT SWNTs enabled an increase in open-circuit voltage from 0.39 to 0.44 V when used as the active material in solar cells. In addition, the external quantum efficiency (EQE) of the solar cell reached 16% at an excitation wavelength of 1020 nm, compared to 4% for HiPco SWNT solar cells at its peak wavelength of 1100 nm.[20,23] Furthermore, sorted small-diameter CoMoCAT SWNT thin film transistor devices demonstrated an average mobility of >1 $cm^2/(V\,s)$ and an average on/off ratio $>10^4$ with excellent uniformity.

RESULTS AND DISCUSSIONS

Improving Yield by Side Chain Modification. The sorting procedure was similar to our previously reported process[14] which involved only a simple sonication followed by a centrifugation step. First, 5 mg of CoMoCATs and 5 mg of polythiophenes were mixed in 25 mL of toluene for the dispersion process. After the sonication and centrifugation steps, a very dark solution was obtained (Figure 1a). Ultraviolet−visible-near infrared (UV−vis-NIR) spectroscopy was used to measure dispersion yield for polymers of various alkyl side chain lengths (where R = 8, 10, 12, 13 shown in Figure 1b). Compared to unsorted SWNTs dispersed in *N*-methyl-2-pyrrolidone (NMP), the peaks representing SWNTs with different chiralities are well resolved in the rr-P3AT dispersions, indicating well dispersed SWNTs. The yields estimated for P3OT (R = 8), P3DT (R = 10), P3DDT (R = 12), and P3TDT (R = 13) sorted SWNTs were 4%, 17%, 25%, and 31%, respectively. These values were derived by comparing the semiconducting E^S_{11} peak resonance areas in the absorption spectrum with those from NMP dispersion with a known SWNT concentration.[15,24] We ruled out the possibility that this increase in dispersion yield was due to the increase in molecular weight of the polymer because the molecular weight of the polymer did not show any particular trend when the length of the side chains were varied from C8 to C13 (Table S1). We previously reported a 20% yield for P3DDT sorting of HiPco SWNTs,[14] where longer side chains also resulted in a higher sorting yield. Additionally, Gomulya *et al.* also observed a similar trend between alkyl side chain length and sorting efficiency for both HiPco and arc-discharged SWNTs in the case of polyfluorene sorted SWNTs.[17] Hence, we can speculate that regardless of the diameters of the SWNTs, polymers with longer side chains generally result in a higher dispersion yield of SWNTs.

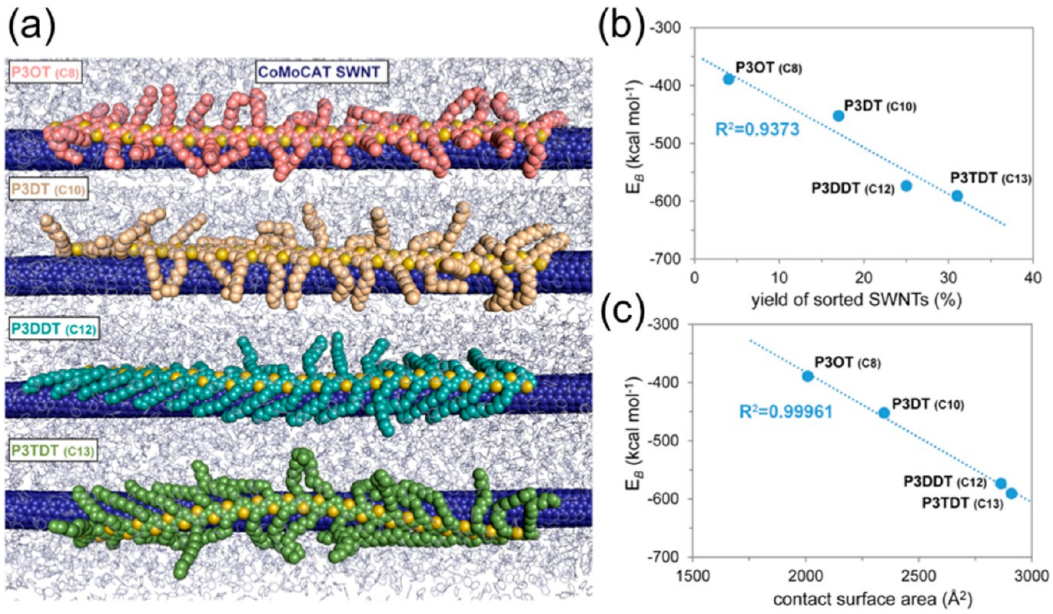

Figure 2. (a) Representative snapshots of the MD simulations for (6,5) SWNT with P3OT, P3DT, P3DDT, and P3TDT in explicit toluene. (b) Calculated binding energies (E_B) *vs* yield of sorted (6,5) SWNTs. (c) Calculated binding energies (E_B) *vs* contact surface area (CSA) between the polythiophene polymers and (6,5) SWNTs. Energies and contact surface areas were averaged along 60 ns MD trajectories. CSA were calculated using UCSF Chimera 1.8.[49]

To investigate the origin of observed increased dispersion yield with increased alkyl side chain length, we performed molecular dynamics (MD) simulations using AMBER 12[26] and the general AMBER force field (GAFF)[27] (see Methods section). The wrapping of four polymer strands (R = 8, 10, 12 and 13; each with 32 repeating units) to a 30 nm long (6,5) nanotube was first simulated for 100 ns in implicit toluene (*i.e.*, bulk solvent treated as a dielectric continuum with $\varepsilon = 2.84$). Then, an additional 60 ns simulation in explicit toluene (*i.e.*, polymer/SWNT complex immersed in a periodic box of toluene molecules) was performed to account for the interactions between the polymer and the solvent molecules.[17] During the initial stages of the implicit solvation simulation, the polymer backbones gradually evolved from a linear arrangement to a more helical wrapping around the circumference of the nanotube. After approximately 200 ps, the polymer backbone extended to a more stable quasi-linear conformation and remained in contact with the nanotube surface. Previous MD studies by Grossman,[25] Mattoni,[26] and our own work[15] indicated similar phenomena in the polymer wrapping process with SWNTs. A greater propensity for formation of helical conformations of the polymer backbones was observed when the simulations were performed in explicit solvent. Strong contact of the alkyl side chains with the nanotube surface was observed throughout the simulations since most alkyl side chains remained bound to the nanotube surface. Snapshots of the structures of the polymers interacting with (6,5) SWNT obtained after 60 ns simulation in explicit solvent are shown in Figure 2a. The flexibility of the polythiophene backbone and the alkyl side chains, together with the good line-up of the alkyl side chains due to the regioregularity, collectively resulted in the tight wrapping of the polymer to the curved nanotube surface.

We computed the binding energy (E_B) of the SWNT/polythiophene complex as follows: $E_B = [E_{complex} - (E_{SWNT} + E_{polythiophene})]$, where $E_{complex}$, E_{SWNT}, and $E_{polythiophene}$ are the energies of the SWNT/polythiophene complex, the nanotube, and the polymer, respectively, based on the implicit generalized Born (GB) solvation model.[27] The computed average binding energies during the 60 ns explicit solvation simulation of the four different polymers with (6,5) SWNT are shown in Figure 2. During this period, when the systems were completely equilibrated, the average binding energies of P3DDT (C12) and P3TDT (C13) with (6,5) CoMoCAT SWNT were similar and the greatest among the four polymers. This observation is in agreement with the measured amounts of SWNTs dispersed (Figure 2b).

The origin of the greater binding energies of the P3DDT and P3TDT polymers was attributed to their longer side chains, which led to higher contact surface area (CSA) for the same length of polymer and thus promoted the binding with the nanotubes. For all the polymers studied, the computed binding energies correlated well with the CSA (Figure 2c). Similar correlations of the polymer/SWNT contact surface area and binding energies were observed in our previous molecular dynamics studies of dithiafulvalene/thiophene copolymer wrapping of SWNT.[15] These results were in agreement with our previously reported hypothesis that the side chain/SWNT interactions promoted polymer/SWNT binding and contributed to the observed selectivity in sorting of the nanotubes.[15]

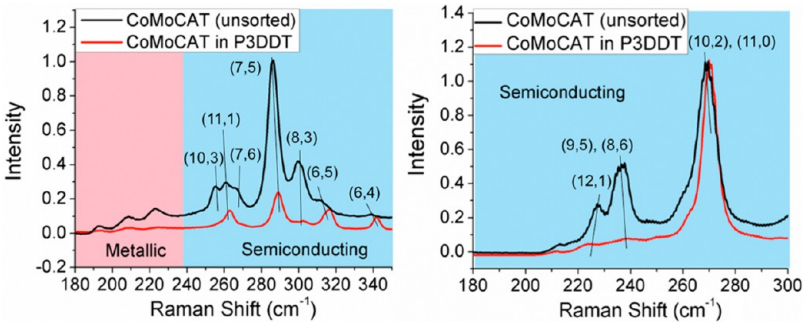

Figure 3. Raman spectra of unsorted CoMoCAT SWNTs dispersed by NMP and sorted ones dispersed by P3DDT: (a) with 633 nm laser excitation (b) with 785 nm laser excitation.

Another factor that might have contributed to the efficient SWNT dispersion by polymers with longer alkyl side chains is that the stronger side chain/solvent interactions lead to increased solubility of the wrapped SWNT in toluene. To explore whether the longer alkyl side chains in the wrapped SWNT indeed interact more favorably with the solvent molecules than with SWNT surface, we compared the geometries and binding energies of the polymer/SWNT complexes with and without explicit toluene solvent molecules. When solvated and equilibrated in toluene, the side chain interactions with solvent molecules increased noticeably, leading to a decrease of polymer/SWNT CSA and binding energy compared to the values obtained from implicit solvation simulations (Figure S1). The SWNT/polymer binding energies in explicit solvent (E_B) decreased by approximately 3−4 kcal mol^{-1} per monomer unit (Figure S1). Surprisingly, the effect of explicit solvation on binding energy and CSA was more significant for polymers with short alkyl chains than those with the long ones. The binding energies of P3OT and P3DT to SWNT decreased 22−23% when explicit solvent was considered. In contrast, the binding energies of P3DDT and P3TDT only decreased 14−15% in explicit solution. Similarly, the CSA also decreased more with the shorter side chain polymers (18−21% for P3OT and P3DT, and 8−9% for P3DDT and P3TDT). As depicted in the representative structures, the shorter alkyl groups appeared to solvate better in toluene in comparison to implicit solvent (Figure 2a and S2c). This observation is somewhat counterintuitive and has been observed for high molecular weight alkanes.[27] Longer alkyl chains seemed to have a larger SWNT/toluene partition coefficient than the shorter chains. These results reinforce the notion that the origin of greater SWNT dispersion yield with polymers with long alkyl side chains is the stronger interactions of these peripheral residues with the nanotubes, achieving more effective wrapping of SWNTs. The principle of increasing the CSA between the polymers and nanotubes is highly applicable to design more efficient polymers for sorting SWNT dispersion.

Selective Dispersion of Small-Diameter SWNTs. The sorting selectivity of the CoMoCAT SWNTs by rr-P3AT polymers was characterized by UV−vis-NIR, Raman resonance spectroscopy and photoluminescence measurements. First, as seen in the UV−vis-NIR spectrum shown in Figure 1b, we observed identical peak positions and similar relative selectivity for SWNTs sorted by polymers with different side chain lengths. In comparison with unsorted SWNTs in NMP, we observed that the absorption peaks for (7,5) and (7,6) SWNTs at a wavelength of 634 nm were largely suppressed, while new features appeared in the sorted SWNTs, *e.g.*, a small (9,1) peak at 975 nm. To compare the selectivity of polymers with different side chain lengths, the absorption spectra for polymers with different alkyl chain lengths were normalized to (6,5) peak as shown in Figure S2. We observed that the polymers with longer alkyl side chains are slightly less selective to SWNTs because their higher contact surface area allows them to bind with more types of SWNTs. Since polymers with different alkyl chain lengths varied so little in their selectivity toward SWNTs, the CoMoCAT SWNTs sorted by commercially available P3DDT will be examined further as an example for their composition and device performance.

With the use of Raman spectroscopy, major peaks of CoMoCAT SWNTs were probed with lasers excitation energies of 1.96 eV (633 nm) and 1.58 eV (785 nm). The radial breathing mode (RBM) of the SWNTs selected before and after sorting by P3DDT is shown in Figure 3. When the SWNTs were irradiated using the 633 nm laser, we observed that the peaks of the metallic SWNTs that were originally present in the unsorted SWNTs were almost completely eliminated after sorting. In the regime for semiconducting SWNT resonance, the peaks for (10,3), (11,1), (7,6), (7,5), and (8,3) SWNTs were all suppressed, which is consistent with the reduction of (7,5) and (7,6) peaks observed by UV−vis-NIR measurements. On the other hand, the smallest diameter (6,5) and (6,4) SWNT peaks were clearly enriched as evidenced from the increased relative intensity. With the 785 nm laser excitation, the peaks of the relatively larger-diameter (8,6), (9,5), and (12,1) SWNTs were also suppressed significantly after the sorting process. In comparison with (8,6)/(9,5) peaks in UV−vis-NIR spectrum in Figure 1c, the reduction of (8,6)/(9,5) peaks at Raman 785 nm laser are much

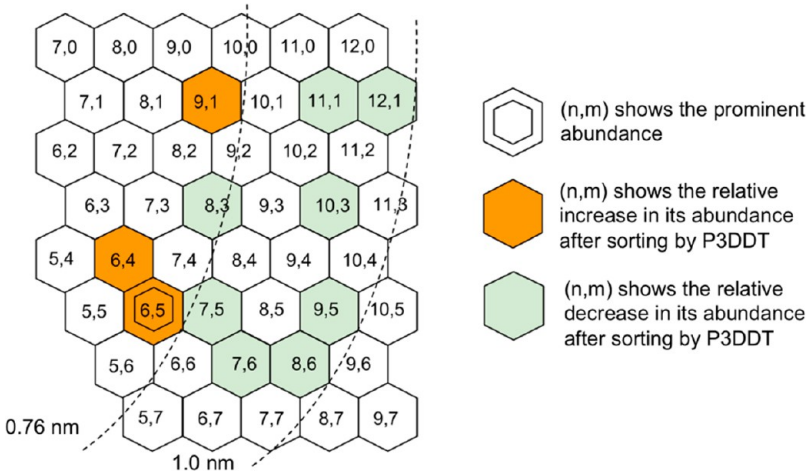

Figure 4. Sorted Chirality Map showing the enrichment of CoMoCAT SWNTs by P3DDT: orange hexagons and light green circles are showing the increase or decrease in the abundance of SWNTs after sorting with P3DDT, respectively, from UV−vis-NIR and Raman spectroscopy.

more distinct. This discrepancy might be due to the residue burned polymers that shift the optical transitions of the SWNTs outside the resonance range of the Raman excitation lasers. It was reported that both induced strain[28] or dielectric screening[29] could shift the optical transition energies of SWNTs. The photoluminescence measurements presented in Figure S3 also demonstrated the predominance of small-diameter (6,5) species in the P3DDT sorted SWNT solutions.

Using the UV−vis-NIR and Raman spectroscopy features, we summarize the enrichment of the semiconducting CoMoCAT SWNT species in the Sorted Chirality Map shown in Figure 4. The orange hexagons represent the relative enrichment in SWNT types, while the light green hexagons represent the relative reduction in SWNT types. The polythiophene polymer sorting process clearly dispersed semiconducting SWNTs with diameter <0.76 nm, which are the smallest-diameter species among all the CoMoCAT SWNTs. In comparison with selecting larger-diameter SWNTs with dithiafulvalene/thiophene copolymers previously,[15] the preferred extraction of small-diameter of SWNTs by P3DDT in this work might be due to the lack of fused aromatic rings in the P3DDT backbone, which allows the polymer to adapt a more curved conformation for achieving a better wrapping with higher curvature, smaller-diameter SWNTs. Fortunately, the selected SWNTs possess first interband transition (S11) larger than 1.1 eV, which correspond to desirable bandgaps for materials integrated in a solar cell. In fact, the optimal bandgap for a single junction photovoltaic cell is 1.3 eV considering the Shockley-Queisser limit.[30]

Photovoltaic Device. SWNTs have previously been employed as donors in bilayer solar cell architectures.[7−9,20,23,31,32] Specifically, polymer-sorted SWNTs achieved higher performance due to the near complete removal of metallic SWNTs in the active layers, which can cause direct shorting of the device and quenching of excitons.[25,26] Ideally, the active layer of an organic solar cell comprises a combination of donor and acceptor materials engineered such that:

(1) Their energy levels are aligned to form a type II heterojunction.[33] In general, the energy offset between the LUMO level of the donor and that of the acceptor directly influences the exciton separation efficiency, while the difference between the LUMO of the acceptor and the HOMO of the donor relates directly to the upper-limit of the open circuit voltage.

(2) They typically absorb complementing regions of the AM1.5 solar spectrum to maximize the photons that can be potentially harvested in the solar cell.

In principle, our rr-P3DDT sorted CoMoCAT SWNTs, in conjunction with C_{60}, is able to satisfy the above requirements better than our previously reported rr-P3DDT sorted HiPco SWNTs.[8] As shown in Figure 5a, the CoMoCAT SWNTs film possesses absorption peaks closer to the 1.3 eV bandgap (~950 nm) than the HiPco SWNTs, which have peaks up to 0.85 eV (~1450 nm). By employing the heterojunction structure in all our devices, we proceed to evaluate the contribution of the sorted CoMoCAT SWNTs to the overall efficiency in comparison with the sorted HiPco SWNTs.

The active layer consists of a bilayer of 70 nm of C_{60} on top of a spincoated thin layer of SWNTs (~3−5 nm thick). We used ITO as the anode and poly(3,4-ethylenedoxythiophene):poly(styrenesulfonate) (PEDOT:PSS) layer as a hole transporting layer. 70 nm of Ag was used as the top reflective cathode. We present an AFM image of the rr-P3DDT dispersed CoMoCAT spin-coated film in Figure 5b, and both the schematic of the device structure and the corresponding energy band level diagrams are shown in Figure 5, panels c and d, respectively.

As depicted in Figure 5e, CoMoCAT SWNTs based solar cells exhibited systematically higher open circuit voltages of 0.44 V, compared to the 0.39 V open circuit

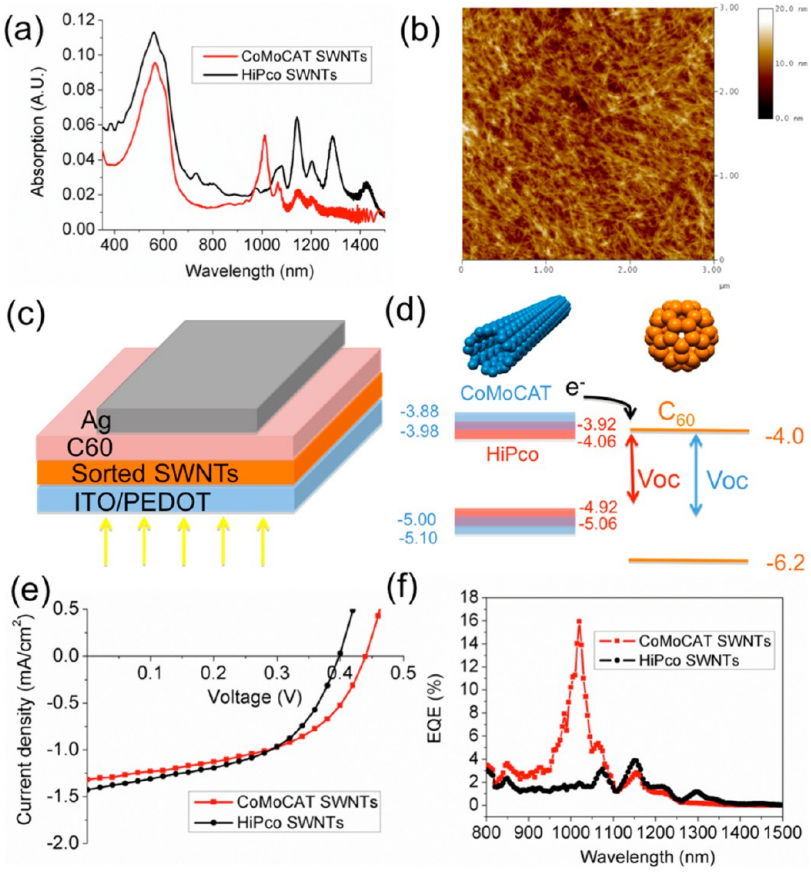

Figure 5. (a) Comparison of the UV−vis-NIR absorption spectra between P3DDT sorted CoMoCAT and HiPco SWNTs films. (b) AFM image of the sorted CoMoCAT SWNTs layer. (c) Device structure of the carbon based solar cell structure. (d) Schematic diagram showing the band structure (the numbers are theoretical HOMO and LUMO range of first von Hove singularities for both HiPco and CoMoCAT SWNTs respectively estimated according to the same method as Tange *et al.*[16]), predicted open circuit voltage and charge transfer of SWNTs/C_{60} heterojunction. (e) *J*−*V* characteristics of the devices measured under simulated AM1.5 solar illumination for CoMoCAT SWNTs and HipCO SWNTs dispersed by P3DDT. (f) External quantum efficiency for the comparison of HiPco and CoMoCAT SWNTs in the IR regime.

voltage of solar cells fabricated from HiPco SWNTs. We attributed this increase in open circuit voltage to the smaller diameter and lower bandgap tubes in the sorted CoMoCAT SWNTs. The open circuit voltage is generally related to the difference between the HOMO of SWNTs and the LUMO of C_{60}, which are labeled in Figure 5d.

As mentioned previously, employing CoMoCAT SWNTs in solar cells should enable a more efficient charge separation which should be directly translated into a higher short-circuit current. However, as depicted in the *J*−*V* curve (Figure 5e), we observed that the currents generated from both types of solar cells are approximately equivalent. We thus analyzed the amount of infrared and visible photons absorbed by the SWNTs and the polymers, respectively, in the solar cells and compared it to the amount of charges they each contributed to the current (Figure 5e,f).

In Figure 5a, we observed that the 5 nm thick P3DDT wrapped HiPco SWNTs films had higher absorption peak intensities not only in the near-infrared (at 1150 nm), but also in the visible at 550 nm indicating a slightly higher polymer content in the spin-coated films. Thus, for HiPco based solar cells, the current generated is dominated by the contribution of the P3DDT absorption in the visible,[8] rather than the infrared contribution of the SWNTs. On the other hand, for the CoMoCAT based films, there was a significant contribution from the SWNTs due to the more efficient charge transfer from the small diameter SWNTs to the C_{60} (larger LUMO offsets between SWNTs and C_{60}), which was further highlighted by the high EQE peak of 16% at 1050 nm (Figure 5f). We clearly observed a lower near-infrared carrier separation efficiency from the large diameter HiPco SWNTs to the C_{60} with the EQE peaks at 1100 nm being suppressed reaching a maximum of only 4% and the peaks above 1200 nm almost completely eliminated. Arnold *et al.* previously reported EQE peaks higher than 30% at 1050 nm from PFO sorted (7,5) CoMoCAT based solar cells.[20,34] Their higher EQE value may be due to the inclusion of a buffer layer to minimize charge recombination and the use of optimized thickness for their SWNT film to maximize interference effects at 1050 nm. Interestingly, the V_{oc} (0.44 V) of our device is higher than their V_{oc} of 0.38 V under simulated AM1.5 solar illumination.[34] This result was due to our utilization of sorted CoMoCAT tubes,

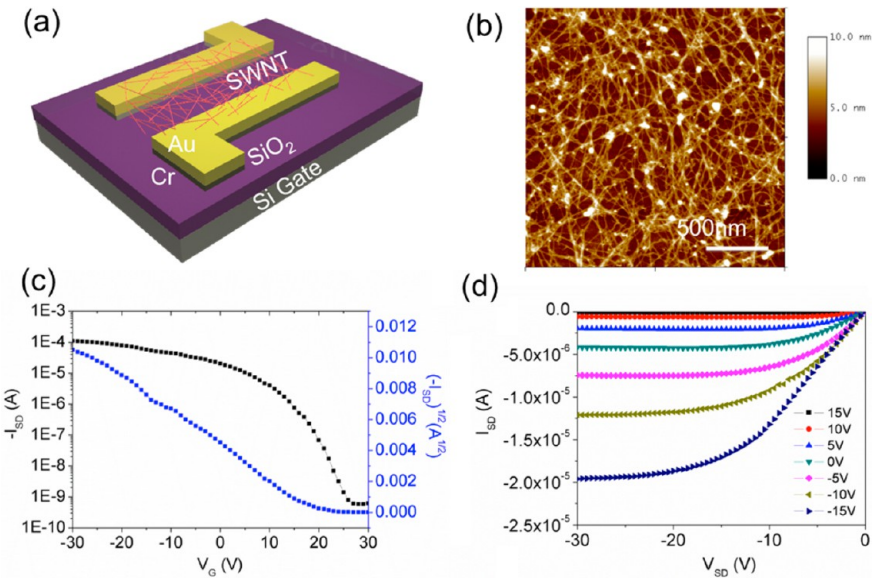

Figure 6. Electrical transport properties of thin film transistors made of P3DDT dispersed CoMoCAT SWNTs in toluene: (a) schematic diagram of the device structure (L = 20 μm, W = 400 μm); (b) AFM image of P3DDT sorted CoMoCAT SWNTs; (c) transfer curve of a typical device (V_{SD} = −30 V); (d) output curve of the device in (c) at different gate voltages.

predominantly (6,5) rather than the (7,5), which highlights the benefit of using even smaller diameter SWNTs.

Thin Film Transistors. We successfully demonstrated the merits of our rr-P3DDT sorted CoMoCAT SWNTs for solar cell applications. In this section, we applied these tubes for thin film transistor applications. We fabricated bottom-gate bottom-contact thin film transistors (TFTs) with highly doped silicon substrate as a gate and 300 nm SiO_2 as the dielectric with the sorted CoMoCAT SWNTs. The device structure is shown in Figure 6a and an AFM image of the SWNT films in the channel is shown in Figure 6b. The transfer and output curves of a typical device are shown in Figure 6c,d. Our fabricated devices were observed to exhibit excellent uniformity and have an average charge carrier mobility of 1.18 ± 0.28 $cm^2/(V\ s)$ and average on/off ratio of (2.36 ± 4.52) × 10^4, as computed from more than 20 randomly chosen devices. The high on/off ratio (Histogram of on/off ratios shown in Figure S4) at this high SWNT density (Figure 6b) also supports the high selectivity of the semiconducting SWNTs by polymers. The mobility of this SWNT-film is also in the same order of magnitude as compared to PFO sorted CoMoCAT[35] or even some of the larger-diameter SWNT TFTs[15,36] using similar device architectures. For random network SWNT TFTs, the contact between the small-diameter SWNTs and metals is not the limiting factor as is the case for single SWNT devices.[19] Indeed, we observed negligible contact resistances as shown from the output curves in Figure 6d. Rather, the limiting factor of our thin-film transistor can be attributed to tube-to-tube junctions between the SWNTs, which under percolation transport have been shown to dominate the resistance of the channel.[37] Therefore, by implement alignment techniques to optimally set the tube-to-tube junctions or by reducing the tube-to-tube junction resistance can potentially improve the performance of our transistor.

CONCLUSION

In summary, we have demonstrated the enrichment of smaller-diameter semiconducting SWNTs from CoMoCAT SWNTs using simple sonication and centrifugation processes. We observed that the yield of dispersion increased upon the lengthening of polymer's alkyl side chain. Molecular dynamics simulations indicated that the stronger interaction is due to the higher surface contact area between the longer alkyl side chain of the polymers and the SWNT. We also demonstrated that the sorted, highly concentrated smaller-diameter, wider bandgap CoMoCAT SWNTs have great potential in solar cell applications, due to their improved open-circuit voltage and their improved near-infrared carrier extraction over the sorted HiPco SWNTs. Finally, thin film transistors fabricated with our sorted CoMoCAT SWNTs demonstrated excellent uniformity, mobility and on/off ratio. The high charge carrier mobility, together with the improved charge extraction efficiency, indicates that it would be highly advantageous to employ polymer sorted small-diameter SWNTs for photovoltaic applications.

METHODS

Preparation of SWNTs Solution. Five milligrams of CoMoCAT SWNTs from Sigma-Alrich was mixed with 5 mg of rr-P3ATs in 25 mL of toluene and sonicated (Cole Parmer ultrasonic processor 750 W) for 30 min at an amplitude level of 70%. The solution was then centrifuged (Sorvall RC5C-plus) at 17 000 rpm

for 1 h at 16 °C. The supernatant was collected and diluted to 1:10 with toluene before making devices. Two milligrams of CoMoCAT SWNTs was sonicated in 10 mL of NMP for UV−vis-NIR measurements to compare the yields of polymer sorting.

SWNTs Structure Characterization. AFM images were taken using tapping mode with a Veeco AFM. Electrical measurements were carried out using a Keithley 4200 SC semiconductor analyzer. Raman spectra were obtained using a confocal Raman system LabRam Aramis from Horiba Jobin Yvon at 633 nm (1.96 eV) and 785 nm (1.58 eV) excitation at 100× magnification, 1 μm spot size, and 1800 grating and 5 mV excitation power. The SWNT solution was drop casted on 300 nm silicon dioxide and was subsequently annealed at 500 °C for 1 h in an Ar atmosphere to remove the polymers.[14] Data was taken by as an average of multiple points mapping (9 points) for two substrates. Each point was an average of 3 spectra. The spectrum was normalized to the 521 cm^{-1} silicon peak. The UV−vis-NIR measurements were done in 1-mm path-length quartz cells by using a Cary 6000i spectrophotometer (Varian) with toluene as a background.

Molecular Dynamics Simulations. The simulations were performed using AMBER 12[38] and the general AMBER force field (GAFF).[39] The partial charges sets for the polymers were generated within the *antechamber* module of AMBER 12 by fitting the electrostatic potential of the monomeric repeating units generated at the HF/6-31G(d) level by the RESP model.[40] The charges were calculated according to the Merz−Singh−Kollman scheme[41,42] using Gaussian 09.[43] The partial charges of the nanotube carbon atoms were set to zero. A 30 nm long nanotube and a regioregular polymer strand with 32 repeating units (n = 32) were employed in each simulation. The starting structures for the MD simulations consisted of the planar configuration of the four polymers situated *ca.* 5 Å from the nanotube surface at an angle of *ca.* 45° with respect to the nanotube. The simulation conditions in implicit solvent for the initial wrapping process (100 ns) were the same used in our previous study.[15] For the simulations in explicit solvent, each wrapped polymer/nanotube complex derived from the initial simulations in implicit solvent was immersed in a pre-equilibrated truncated octahedral box of toluene molecules[44] with an internal offset distance of 20 Å, using the *leap* module,[45] which resulted in the addition of around 4200 solvent molecules. All systems were neutral, and thus no explicit counterions were added. A two-stage geometry optimization approach was performed prior to the explicit solvation simulation. First, a short minimization of the toluene molecules positions, with positional restraints on solute by a harmonic potential with a force constant of 500 kcal mol^{-1} $Å^{-2}$ was performed. The second stage was an unrestrained minimization of all the atoms in the simulation cell. Then, the systems were gently heated (0−300 K) under constant-volume, periodic-boundary conditions and the particle-mesh Ewald approach[46] to introduce long-range electrostatic effects. For this and the subsequent steps, an 8 Å cutoff was applied to Lennard-Jones and electrostatic interactions. Bonds involving hydrogen were constrained with the Shake algorithm.[47] Harmonic restraints of 10 kcal mol^{-1} were applied to the solute, and the Andersen equilibration scheme was used to control and equalize the temperature.[48] The time step was kept at 1 fs during all stages of the simulation, allowing potential inhomogeneities to self-adjust. Each system was then equilibrated without restrains for 250 ps at a constant pressure of 1 atm, and for 500 ps at constant volume. Finally, a 60 ns unrestrained MD trajectory at constant volume and temperature (300 K) was collected and analyzed using the *ptraj* module.

Solar Cell Fabrication and Characterization. Clean, patterned ITO (~15 Ω/sq) on glass was used as the substrate. The substrates were treated with 15 min of UV−O_3; then, a PEDOT:PSS solution (CLEVIOS AL4083, Heraeus) was spin-coated on the substrates at 3000 rpm for 1 min followed by annealing at 120 °C for 30 min. The substrates were then transferred to an N_2 environment for SWNT deposition. SWNT solutions were spin-coated at 700 rpm for 30 s followed by 4000 rpm for 10 s. This process was repeated 5 times with a 2-min annealing step at 100 °C to remove excess solvent. After SWNT deposition, 70 nm commercially available C_{60} (Fullerene Powder, sublimed, 99.9+%, Alfa Aesar) was deposited thermally under vacuum (5×10^{-5} Torr) at 0.05 nm/s (Angstrom Engineering evaporator). Similarly, 70 nm of Ag was vacuum evaporated on top of the C_{60} at 0.05 nm/s (Thermionics Laboratory, Inc. evaporator). Solar spectra were obtained with a Newport solar simulator with a flux of 100 mW/cm^2 that approximated the solar spectrum under AM1.5G conditions in an N_2 environment. The area of the devices was 0.04 cm^2.

Transistor Fabrication and Electrical Characterization. The drain and source electrodes for bottom-contact devices electrodes were fabricated on highly doped 4 in. silicon wafer with 300 nm SiO_2 by photolithography. A bilayer of Cr (5 nm) and Au (40 nm) was deposited by thermal evaporation as the source-drain electrodes, followed by a lift-off process in acetone. The substrate was then soaked in the (1:20 ratio) diluted solution of sorted SWNTs for 16 h. A Keithley 4200 SC semiconductor analyzer was used to measure the electrical properties of the devices. Source-drain voltage (V_{SD}) of −40 V is used for all the reported measurements.

Conflict of Interest: The authors declare no competing financial interest.

Supporting Information Available: Calculated E_B *vs* yield of sorted (6,5) SWNTs and *vs* CSA; absorption spectra for polymers with different alkyl chain lengths normalized to (6,5) peak; photoluminescence measurements; histogram of on/off ratios of the P3DDT sorted CoMoCAT transistors; table listing molecular weight and polydispersity values for different polymers measured by GPC. This material is available free of charge *via* the Internet at http://pubs.acs.org.

Acknowledgment. This work was funded by Global Climate and Energy Project (GCEP) at Stanford University, National Science Foundation (Award Number: 1059020 and 1335645) and the Air Force office of Scientific Research (FA9550-12-1-0190). H.W. acknowledges financial support from Link foundation Energy fellowship. G.I.K. acknowledges the support of the Government of Canada and the Natural Sciences and Engineering Research Council of Canada (NSERC) in the form of the Banting Postdoctoral Fellowship. Y.-C.L. thanks his supporting funding from Taiwan National Science Council (102-2917-i-002-087).

REFERENCES AND NOTES

1. Dürkop, T.; Getty, S. A.; Cobas, E.; Fuhrer, M. S. Extraordinary Mobility in Semiconducting Carbon Nanotubes. *Nano Lett.* **2003**, *4*, 35–39.
2. Wang, H.; Luo, J.; Robertson, A.; Ito, Y.; Yan, W.; Lang, V.; Zaka, M.; Schäffel, F.; Rümmeli, M. H.; Briggs, G. A. D.; Warner, J. H. High-Performance Field Effect Transistors from Solution Processed Carbon Nanotubes. *ACS Nano* **2010**, *4*, 6659–6664.
3. Avouris, P.; Freitag, M.; Perebeinos, V. Carbon-Nanotube Photonics and Optoelectronics. *Nat. Photonics* **2008**, *2*, 341–350.
4. LeMieux, M. C.; Roberts, M.; Barman, S.; Jin, Y. W.; Kim, J. M.; Bao, Z. N. Self-Sorted, Aligned Nanotube Networks for Thin-Film Transistors. *Science* **2008**, *321*, 101–104.
5. Wang, C.; Zhang, J.; Ryu, K.; Badmaev, A.; De Arco, L. G.; Zhou, C. Wafer-Scale Fabrication of Separated Carbon Nanotube Thin-Film Transistors for Display Applications. *Nano Lett.* **2009**, *9*, 4285–4291.
6. Cao, Q.; Kim, H. S.; Pimparkar, N.; Kulkarni, J. P.; Wang, C.; Shim, M.; Roy, K.; Alam, M. A.; Rogers, J. A. Medium-Scale Carbon Manotube Thin-Film Integrated Circuits on Flexible Plastic Substrates. *Nature* **2008**, *454*, 495–500.
7. Tung, V. C.; Huang, J. H.; Kim, J.; Smith, A. J.; Chu, C. W.; Huang, J. Towards Solution Processed All-Carbon Solar Cells: A perspective. *Energy Environ. Sci.* **2012**, *5*, 7810–7818.
8. Ramuz, M. P.; Vosgueritchian, M.; Wei, P.; Wang, C.; Gao, Y.; Wu, Y.; Chen, Y.; Bao, Z. Evaluation of Solution-Processable Carbon-Based Electrodes for All-Carbon Solar Cells. *ACS Nano* **2012**, *6*, 10384–10395.
9. Arnold, M. S.; Zimmerman, J. D.; Renshaw, C. K.; Xu, X.; Lunt, R. R.; Austin, C. M.; Forrest, S. R. Broad Spectral Response Using Carbon Nanotube/Organic Semiconductor/C60 Photodetectors. *Nano Lett.* **2009**, *9*, 3354–3358.

10. Arnold, M. S.; Green, A. A.; Hulvat, J. F.; Stupp, S. I.; Hersam, M. C. Sorting Carbon Nanotubes by Electronic Structure using Density Differentiation. *Nat. Nanotechnol.* **2006**, *1*, 60–65.
11. Tu, X.; Manohar, S.; Jagota, A.; Zheng, M. DNA Sequence Motifs for Structure-Specific Recognition and Separation of Carbon Manotubes. *Nature* **2009**, *460*, 250–253.
12. Liu, H.; Nishide, D.; Tanaka, T.; Kataura, H. Large-Scale Single-Chirality Separation of Single-Wall Carbon Nanotubes by Simple Gel Chromatography. *Nat. Commun.* **2011**, *2*, No. 309.
13. Nish, A.; Hwang, J. Y.; Doig, J.; Nicholas, R. J. Highly Selective Dispersion of Single-Walled Carbon Nanotubes Using Aromatic Polymers. *Nat. Nanotechnol.* **2007**, *2*, 640–646.
14. Lee, H. W.; Yoon, Y.; Park, S.; Oh, J. H.; Hong, S.; Liyanage, L. S.; Wang, H.; Morishita, S.; Patil, N.; Park, Y. J.; *et al.* Selective Dispersion of High Purity Semiconducting Single-Walled Carbon Nanotubes with Regioregular Poly(3-alkylthiophene)s. *Nat Commun.* **2011**, *2*, 541.
15. Wang, H.; Mei, J.; Liu, P.; Schmidt, K.; Jiménez-Osés, G.; Osuna, S.; Fang, L.; Tassone, C. J.; Zoombelt, A. P.; Sokolov, A. N.; *et al.* Scalable and Selective Dispersion of Semiconducting Arc-Discharged Carbon Nanotubes by Dithiafulvalene/Thiophene Copolymers for Thin Film Transistors. *ACS Nano* **2013**, *7*, 2659–2668.
16. Tange, M.; Okazaki, T.; Iijima, S. Selective Extraction of Large-Diameter Single-Wall Carbon Nanotubes with Specific Chiral Indices by Poly(9,9-dioctylfluorene-alt-benzothiadiazole). *J. Am. Chem. Soc.* **2011**, *133*, 11908–11911.
17. Gomulya, W.; Costanzo, G. D.; De Carvalho, E. J. F.; Bisri, S. Z.; Derenskyi, V.; Fritsch, M.; Fröhlich, N.; Allard, S.; Gordiichuk, P.; Herrmann, A.; *et al.* Semiconducting Single-Walled Carbon Nanotubes on Demand by Polymer Wrapping. *Adv. Mater.* **2013**, *25*, 2948–2956.
18. Zhou, X.; Park, J.-Y.; Huang, S.; Liu, J.; McEuen, P. L. Band Structure, Phonon Scattering, and the Performance Limit of Single-Walled Carbon Nanotube Transistors. *Phy. Rev. Lett.* **2005**, *95*, 146805.
19. Chen, Z.; Appenzeller, J.; Knoch, J.; Lin, Y.-m.; Avouris, P. The Role of Metal−Nanotube Contact in the Performance of Carbon Nanotube Field-Effect Transistors. *Nano Lett.* **2005**, *5*, 1497–1502.
20. Bindl, D. J.; Arnold, M. S. Efficient Exciton Relaxation and Charge Generation in Nearly Monochiral (7,5) Carbon Nanotube/C60 Thin-Film Photovoltaics. *J. Phy. Chem. C* **2013**, *117*, 2390–2395.
21. Stranks, S. D.; Weisspfennig, C.; Parkinson, P.; Johnston, M. B.; Herz, L. M.; Nicholas, R. J. Ultrafast Charge Separation at a Polymer−Single-Walled Carbon Nanotube Molecular Junction. *Nano Lett.* **2010**, *11*, 66–72.
22. Ozawa, H.; Ide, N.; Fujigaya, T.; Niidome, Y.; Nakashima, N. One-pot Separation of Highly Enriched (6,5)-Single-walled Carbon Nanotubes Using a Fluorene-based Copolymer. *Chem. Lett.* **2011**, *40*, 239–241.
23. Jain, R. M.; Howden, R.; Tvrdy, K.; Shimizu, S.; Hilmer, A. J.; McNicholas, T. P.; Gleason, K. K.; Strano, M. S. Polymer-Free Near-Infrared Photovoltaics with Single Chirality (6,5) Semiconducting Carbon Nanotube Active Layers. *Adv. Mater.* **2012**, *24*, 4436–4439.
24. Tan, Y.; Resasco, D. E. Dispersion of Single-Walled Carbon Nanotubes of Narrow Diameter Distribution. *J. Phy. Chem. B* **2005**, *109*, 14454–14460.
25. Bernardi, M.; Giulianini, M.; Grossman, J. C. Self-Assembly and Its Impact on Interfacial Charge Transfer in Carbon Nanotube/P3HT Solar Cells. *ACS Nano* **2010**, *4*, 6599–6606.
26. Caddeo, C.; Melis, C.; Colombo, L.; Mattoni, A. Understanding the Helical Wrapping of Poly(3-hexylthiophene) on Carbon Nanotubes. *J. Phys. Chem. C* **2010**, *114*, 21109–21113.
27. Tsui, V.; Case, D. A. Theory and Applications of the Generalized Born Solvation Model in Macromolecular Simulations. *Biopolymers* **2000**, *56*, 275–291.
28. Tange, M.; Okazaki, T.; Iijima, S. Influence of Structure-Selective Fluorene-Based Polymer Wrapping on Optical Transitions of Single-Wall Carbon Nanotubes. *Nanoscale* **2014**, *6*, 248–254.
29. Ferguson, A. J.; Blackburn, J. L.; Holt, J. M.; Kopidakis, N.; Tenent, R. C.; Barnes, T. M.; Heben, M. J. Rumbles, G. Photoinduced Energy and Charge Transfer in P3HT:SWNT Composites. *J. Phys. Chem. C* **2010**, *1*, 2406–2411.
30. Shockley, W.; Queisser, H. J. Detailed Balance Limit of Efficiency of p-n Junction Solar Cells. *J. Appl. Phys.* **1961**, *32*, 510–519.
31. Bindl, D. J.; Wu, M.-Y.; Prehn, F. C.; Arnold, M. S. Efficiently Harvesting Excitons from Electronic Type-Controlled Semiconducting Carbon Nanotube Films. *Nano Lett.* **2010**, *11*, 455–460.
32. Tung, V. C.; Huang, J. H.; Tevis, I.; Kim, F.; Kim, J.; Chu, C. W.; Stupp, S. I.; Huang, J. Surfactant-Free Water-Processable Photoconductive All-Carbon Composite. *J. Am. Chem. Soc.* **2011**, *133*, 4940–4947.
33. Neamen, D. *Semiconductor Physics and Devices*; Irwin: Chicago, IL, 1997; pp 326−367.
34. Shea, M. J.; Arnold, M. S. 1% Solar Cells Derived from Ultrathin Carbon Nanotube Photoabsorbing Films. *Appl. Phys. Lett.* **2013**, *102*, 243101.
35. Bisri, S. Z.; Gao, J.; Derenskyi, V.; Gomulya, W.; Iezhokin, I.; Gordiichuk, P.; Herrmann, A.; Loi, M. A. High Performance Ambipolar Field-Effect Transistor of Random Network Carbon Nanotubes. *Adv. Mater.* **2012**, *24*, 6147–6152.
36. Vosgueritchian, M.; LeMieux, M. C.; Dodge, D.; Bao, Z. Effect of Surface Chemistry on Electronic Properties of Carbon Nanotube Network Thin Film Transistors. *ACS Nano* **2010**, *4*, 6137–6145.
37. Nirmalraj, P. N.; Lyons, P. E.; De, S.; Coleman, J. N.; Boland, J. J. Electrical Connectivity in Single-Walled Carbon Nanotube Networks. *Nano Lett.* **2009**, *9*, 3890–3895.
38. Case, D. A.; Darden, T. A.; Cheatham, T. E., III; Simmerling, C. L.; Wang, J.; Duke, R. E.; Luo, R.; Walker, R. C.; Zhang, W.; Merz, K. M.; Roberts, B. *et al. AMBER 12*; University of California: San Francisco, 2012.
39. Wang, J.; Wolf, R. M.; Caldwell, J. W.; Kollman, P. A.; Case, D. A. Development and Testing of a General Amber Force Field. *J. Comput. Chem.* **2004**, *25*, 1157–1174.
40. Bayly, C. I.; Cieplak, P.; Cornell, W.; Kollman, P. A. A well-behaved Electrostatic Potential Based Method Using Charge Restraints for Deriving Atomic Charges: the RESP Model. *J. Phys. Chem.* **1993**, *97*, 10269–10280.
41. Besler, B. H.; Merz, K. M.; Kollman, P. A. Atomic Charges Derived from Semiempirical Methods. *J. Comput. Chem.* **1990**, *11*, 431–439.
42. Singh, U. C.; Kollman, P. A. An Approach to Computing Electrostatic Charges for Molecules. *J. Comput. Chem.* **1984**, *5*, 129–145.
43. Frisch, M. J.; Trucks, G. W.; Schlegel, H. B.; Scuseria, G. E.; Robb, M. A.; Cheeseman, J. R.; Scalmani, G.; Barone, V.; Mennucci, B.; Petersson, G. A. *et al.*; *Gaussian 09*, Revision D.01; Gaussian, Inc.: Wallingford, CT, 2009.
44. Baker, C. M.; Grant, G. H. Modeling Aromatic Liquids: Toluene, Phenol, and Pyridine. *J. Chem. Theory Comput.* **2007**, *3*, 530–548.
45. Schafmeister, C. E. A. F.; Ross, W. S.; Romanovski, V. *LEAP*; University of California, San Francisco, 1995.
46. Sagui, C.; Darden, T. A. Molecular Dynamics Simulations of Biomolecules: Long-Range Electrostatic Effects. *Annu. Rev. Biophys. Biomol. Struct.* **1999**, *28*, 155–179.
47. Ryckaert, J.-P.; Ciccotti, G.; Berendsen, H. J. C. Numerical Integration of the Cartesian Equations of Motion of a System with Constraints: Molecular Dynamics of n-Alkanes. *J. Comput. Phys.* **1977**, *23*, 327–341.
48. Andrea, T. A.; Swope, W. C.; Andersen, H. C. The Role of Long Ranged Forces in Determining the Structure and Properties of Liquid Water. *J. Chem. Phys.* **1983**, *79*, 4576–4584.
49. Pettersen, E. F.; Goddard, T. D.; Huang, C. C.; Couch, G. S.; Greenblatt, D. M.; Meng, E. C.; Ferrin, T. E. UCSF Chimera—A Visualization System for Exploratory Research and Analysis. *J. Comput. Chem.* **2004**, *25*, 1605–1612.